Coherent Ionization of Atoms by Dense Beams of Extreme Relativistic Electrons

S. Kim, C. Müller, and A. B. Voitkiv
Institute for Theoretical Physics I, Heinrich-Heine-University Düsseldorf, Universitätsstrasse 1, D-40225 Düsseldorf, Germany

(Received 25 August 2025; revised 9 January 2026; accepted 30 April 2026; published 27 May 2026)

Ionization is one of the basic physical processes, occurring when charged particles penetrate atomic matter. Here, we predict a novel ionization mechanism, arising in collisions with very dense and compact beams of extreme relativistic electrons, in which a significant fraction of the beam electrons acts coherently as a single "superprojectile." We compare this mechanism with the tunnel and overbarrier ionization and ionization by individual electrons, demonstrating that it can strongly dominate the ionization process. We also show that this mechanism and the tunnel ionization are very sensitive to the spatiotemporal structure of the beam that can be used for analyzing the beam properties.

DOI: 10.1103/knz2-4fw4

Electron beams are of great importance for many branches of science. An especially crucial role is played by such beams in physics, where they find a large variety of applications (e.g., for probing subatomic particles [1–3], studying fundamental forces and testing quantum field theories [4], for probing atomic dynamics on an attosecond timescale [5], for generating intense, coherent x-rays [6,7], and in diagnostics of plasma [8]).

Beams of extreme relativistic electrons, which move with a velocity v practically equal to the speed of light c, are crucial in cutting-edge physical research [4]. Until recently, the densities of high-energy electron beams were relatively low and the typical time interval Δt between two consecutive collisions of the beam electrons with the target atom (or nucleus) greatly exceeded the typical target transition time τ. As a result, in collisions with atomic and nuclear targets, the beam acted as a set of individual electrons whose contributions to target cross sections and transition rates add incoherently.

However, highly relativistic electron beams of unprecedented density and with up to $\approx$10 GeV electron energy are nowadays generated by laser or plasma wakefield accelerators [9–12]. For example, beams of few femtosecond-scale duration with currents of $\gtrsim$50 kA can be produced by laser wakefield accelerators [13], and electron beam spikes of $\sim$100 kA were recently generated at the FACET-II facility [14]. Plasma photocathodes [15–17] may yield ultrabright electron pulses with subfemtosecond duration [16] and nanometer-scale normalized emittances, which could be focused to extreme beam densities and corresponding fields of $\sim 10^{10}$ V/cm [18–22].

For such beams, the condition $\Delta t \gg \tau$ may no longer be fulfilled. Accordingly, more than one (or even many) electrons can simultaneously interact with an atomic target, representing a qualitatively new physical situation.

In this Letter, we introduce a novel ionization mechanism, which we term "*coherent impact ionization*," where a significant fraction of the beam electrons acts as a single "superprojectile," tremendously enhancing the ionization process. We compare it with another coherent mechanism, *the tunnel (or overbarrier) ionization*, and with the "standard" approach to ionization in which beam electrons are assumed to act individually.

We demonstrate that this mechanism can largely outperform the ionization by individual electrons and the tunnel ionization. Our analysis also shows that both coherent ionization mechanisms depend very sensitively (but quite differently) on the beam parameters which can be exploited for diagnostics of the beams, which is important for their envisaged applications, such as, e.g., the generation of coherent x-rays [17,23,24].

Let the target atoms be initially in the ground state and rest in the laboratory frame. In this frame, the beam electrons are incident on the target atoms with a velocity $v \approx c$ along the z axis, $\mathbf{v} = (0, 0, v)$; see Fig. 1. Our consideration will be based on the semiclassical approximation, in which only the atomic electron(s) are treated as quantum particles, whereas the atomic nucleus and the beam electrons are described classically. Moreover, it is assumed that the atomic nucleus is always at rest and the beam electrons move along straight-line trajectories. The former is justified by a large nuclear mass (compared to that of the electron), whereas the latter works excellently because the momentum-energy transfers in the collisions

Published by the American Physical Society under the terms of the Creative Commons Attribution 4.0 International license. Further distribution of this work must maintain attribution to the author(s) and the published article's title, journal citation, and DOI.

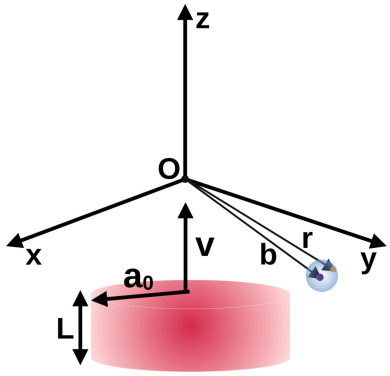


FIG. 1. Sketch of the electron beam-atom collision. The vectors $\boldsymbol{b}$ and $\boldsymbol{r}$ denote the coordinates of the atomic nucleus and the atomic electron, respectively. L, a_0, and $\boldsymbol{v} = (0, 0, v)$ are the beam length, radius, and velocity, respectively. The z axis is also the symmetry axis of the beam.

are negligibly small compared to the momentum and energy of the incident electrons [25].

Let the jth beam electron move along the trajectory $\boldsymbol{R}_j = \boldsymbol{R}_{\perp,j} + \boldsymbol{v}(t - t_j)$, where $\boldsymbol{R}_{\perp,j}$ is its transverse ($\boldsymbol{R}_{\perp,j} \perp \boldsymbol{v}$) coordinate and t_j is the time of its closest approach to the origin. Let the atomic nucleus rest at a point with the coordinates $(\boldsymbol{b}, 0)$, where $\boldsymbol{b} = (b_x, b_y)$ is its transverse position vector, and $\boldsymbol{r} = (x, y, z)$ be the position of the atomic electron with respect to the origin (see Fig. 1).

The electromagnetic field produced by the jth incident electron at the position of the atomic electron can be described by the Lienard-Wiechert potentials:

$$\Phi_j(\boldsymbol{r}, t) = \frac{\gamma e_0}{\sqrt{(\boldsymbol{r}_\perp - \boldsymbol{R}_{\perp,j})^2 + \gamma^2[z - v(t - t_j)]^2}} \tag{1}$$

and $\boldsymbol{A}_j = \boldsymbol{v}/c\Phi_j$ (see, e.g., Ref. [26]), where e_0 is the electron charge, $\gamma = 1/\sqrt{1 - v^2/c^2}$, and $\boldsymbol{r}_\perp = (x, y)$.

Ionization via tunneling and via absorption of high-frequency components from the external field are two facets of the same basic process. Nevertheless, they differ qualitatively and we shall consider them separately, focusing first on the (coherent) impact ionization.

Impact ionization—In collisions of high-energy projectiles with atoms, the overwhelming majority of electrons emitted from the atoms have kinetic energies not significantly exceeding their initial binding energy (see, e.g., Refs. [27,28]). This means that in collisions with light atoms, where bound electrons move with velocities $v_0 \ll c$, the emitted electrons have kinetic energies $\varepsilon \ll m_e c^2$ (m_e is the electron mass). Thus, in such collisions, the atomic electron(s) can be described nonrelativistically.

In collisions with a high-energy electron, the effective strength $\sim e_0^2/\hbar v$ of the perturbation acting on the atom is very weak. Therefore, we shall use the first order of perturbation theory, obtaining for the atomic transition amplitude

$$S_{fi}^j(\boldsymbol{q}_\perp) = -\frac{2i}{\hbar}\frac{e_0^2}{v} e^{iq_\parallel v t_j} e^{-i\boldsymbol{q}_\perp \cdot \boldsymbol{R}_{\perp,j}} \frac{1}{\boldsymbol{q}'^2} \times \left\langle \varphi_f \middle| e^{i\boldsymbol{q}\cdot\boldsymbol{\xi}} - \frac{v}{2m_e c^2}\left(e^{i\boldsymbol{q}\cdot\boldsymbol{\xi}}\hat{p}_z + \hat{p}_z e^{i\boldsymbol{q}\cdot\boldsymbol{\xi}}\right) \middle| \varphi_i \right\rangle. \tag{2}$$

Here, $\boldsymbol{\xi}$ is the coordinate of the atomic electron with respect to the atomic nucleus, φ_i (ε_i) and φ_f (ε_f) are the initial and final states (energies), respectively, of the atomic electron, and $\omega_{fi} = (\varepsilon_f - \varepsilon_i)/\hbar$ is the atomic transition frequency, $\hat{p}_z = (\hbar/i)(\partial/\partial\xi_z)$. Furthermore, $\hbar\boldsymbol{q} = (\hbar\boldsymbol{q}_\perp, \hbar q_\parallel)$ [$\hbar\boldsymbol{q}' = (\hbar\boldsymbol{q}_\perp, \hbar q_\parallel/\gamma)$], where $q_\parallel = \omega_{fi}/v$, is the momentum transferred to the atom in the collision as viewed in the laboratory frame (in the rest frame of the incident electron).

The total transition amplitude is obtained by summing the contributions from all beam electrons:

$$S_{fi}(\boldsymbol{q}_\perp) = -\frac{2i}{\hbar}\frac{e_0^2}{v}\frac{\left\langle \varphi_f \middle| e^{i\boldsymbol{q}\cdot\boldsymbol{\xi}} - \frac{v}{2m_e c^2}\left(e^{i\boldsymbol{q}\cdot\boldsymbol{\xi}}\hat{p}_z + \hat{p}_z e^{i\boldsymbol{q}\cdot\boldsymbol{\xi}}\right) \middle| \varphi_i \right\rangle}{\boldsymbol{q}'^2} \times \sum_{j=1}^{N_t} e^{i(q_\parallel v t_j - \boldsymbol{q}_\perp \cdot \boldsymbol{R}_{\perp,j})}, \tag{3}$$

where N_t is their total number.

From the structure of the amplitude (3), it is obvious that the point of whether more than one electron of the beam may interact coherently with the target depends on the phase factors in the last line in (3).

Let us introduce the longitudinal and transverse coherence lengths, given by $\lambda_\parallel = v/\omega_{fi}$ and $\lambda_\perp = 1/q_\perp$, respectively [29]. $\lambda_\parallel$ represents the distance, which is traversed by the beam electrons during the atomic transition time $1/\omega_{fi}$. Since at $\gamma \gg 1$ the main contribution to the atomic ionization arises in collisions with $q_\perp \ll q_\parallel$ (see, e.g., Ref. [30]), one has $\lambda_\perp \gg \lambda_\parallel$.

Let, further, $\ell_\parallel$ and $\ell_\perp$ be the mean distances between the electrons of the beam in the longitudinal and transverse directions, respectively.

If at least one of the conditions $\lambda_\parallel \ll \ell_\parallel$ and/or $\lambda_\perp \ll \ell_\perp$ is met, the double sum over the beam electrons in $|S_{fi}(\boldsymbol{q}_\perp)|^2$ [arising from the last line in Eq. (3)] reduces to the total number N_t of the electrons in the beam due to their random positions in space. In such a case, the beam interacts with the atom as an incoherent set of individual electrons. This situation represents the "normal" regime in high-energy atomic collisions (and in high-energy physics, in general) and is well studied. In particular, the total cross section σ_t for single ionization by the impact of N_t individual electrons behaves at high energies as

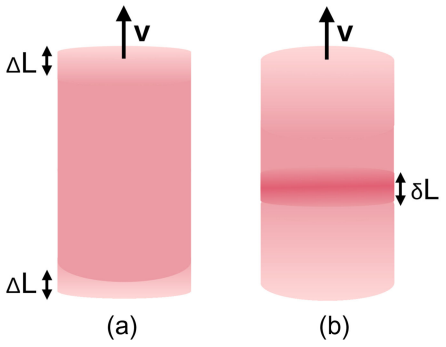


FIG. 2. Sketch of a beam whose intensity (a) "turns on and off" within $\Delta L/v$ and (b) has a spike with duration $\delta L/v$.

$$\sigma_t = N_t \alpha_1 a_B^2 \frac{e_0^4}{\hbar^2 v^2}\left(\ln(\alpha_2 \gamma v/v_B) - 0.5 v^2/c^2\right), \quad (4)$$

where a_B and v_B are the Bohr radius and velocity, respectively, and α_1 and α_2 are dimensionless quantities depending solely on the target atom [31,32].

A qualitatively different collision regime arises when the conditions $\lambda_\parallel \gtrsim \ell_\parallel$ and $\lambda_\perp \gtrsim \ell_\perp$ are fulfilled. Then, the beam no longer acts as a set of individual electrons. Instead, now many electrons from the beam simultaneously interact with the atom, which "sees" the beam essentially as a continuous charge distribution. In such a case, the last line in Eq. (3) is transformed according to

$$\sum_{j=1}^{N_t} e^{i(q_\parallel v t_j - \boldsymbol{q}_\perp \cdot \boldsymbol{R}_{\perp j})} \to \int d^3\boldsymbol{R}\rho(\boldsymbol{R}) e^{-i(q_\parallel Z + \boldsymbol{q}_\perp \cdot \boldsymbol{R}_\perp)}, \quad (5)$$

where $\boldsymbol{R} = (\boldsymbol{R}_\perp, Z)$, ρ is the beam density, and the integration runs over the volume occupied by the beam.

The total cross section for impact ionization $\sigma_{\rm ion}$ reads

$$\sigma_{\rm ion} = \int \frac{d^3\boldsymbol{p} V}{(2\pi\hbar)^3} \int d^2\boldsymbol{q}_\perp |S_{fi}(\boldsymbol{q}_\perp)|^2, \quad (6)$$

where $\boldsymbol{p}$ and V are the momentum and the normalization volume, respectively, of the emitted electron.

As in ionization by individual projectiles, the coherent impact ionization can be viewed as occurring via the absorption of "equivalent photons" [33,34], generated in this case by the concerted action of the beam electrons. Therefore, for this mechanism to be efficient, there must be enough photons with energies greater than the atomic binding energy. This holds if (i) the beam is short, $L \lesssim 10 v\tau$, where τ is the effective target transition time; (ii) the beam is long, but along the propagation direction its density significantly varies over distances $\lesssim 10 v\tau$ (e.g., in its front and/or rear part, or in spikes; see Fig. 2 for an illustration).

Tunnel and overbarrier ionization—When the field, coherently created by the beam electrons, varies slowly on the atomic timescale but is sufficiently strong, the atom is ionized via tunneling [35–37]. For even stronger fields, which are comparable to the internal atomic field or even exceed it, the overbarrier ionization occurs. The tunnel and overbarrier ionization are highly nonperturbative processes, qualitatively different from the (perturbative) impact ionization, which requires sufficiently high-frequency components in the projectile's field but, in general, does not necessitate strong fields.

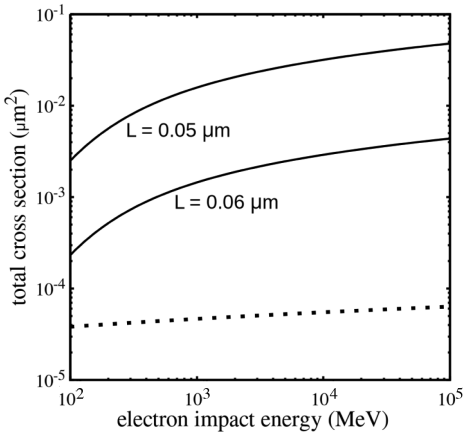


FIG. 3. Single ionization of He$(1s^2)$ atoms by electron beams, as a function of the electron energy. $N_t = 2 \times 10^6$, $a_0 = 1$ μm, and $L = 0.05$ and 0.06 μm, as indicated. Solid curves: the coherent impact ionization. Dotted curve: the cross section (4).

Ionization versus atomic position—An additional insight into the ionization process is obtained by exploring the atomic ionization probability $P_{\rm ion}(b)$ as a function of the atomic position b with respect to the beam axis (see Fig. 1). [We note that the ionization cross sections are given by $2\pi \int_0^\infty dbbP_{\rm ion}(b)$.]

Numerical results and discussion—In Figs. 3 and 4, we show the results for the total cross sections of single ionization of He$(1s^2)$, when a helium gas target is penetrated by beams with electron energy ranging between 100 MeV and 100 GeV ($2 \times 10^2 \lesssim \gamma \lesssim 2 \times 10^5$). The cross sections are given *per beam*.

The results for the coherent impact ionization, shown in Fig. 3, were obtained by taking the beam density as

$$\rho(\boldsymbol{R}, t) = \frac{2N_t}{\pi^{3/2} a_0^2 L} e^{-\eta^2/(L/2)^2} e^{-R_\perp^2/a_0^2}, \quad (7)$$

where $N_t = 2 \times 10^6$, $\eta = Z - vt$, and $a_0 = 1$ μm. Two short beam lengths, 0.05 and 0.06 μm, are considered (the associated beam currents are $\lesssim 2$ kA). The beam pulse time $L/v = 0.167$ and 0.2 fs can be compared to the effective target transition time $\tau \approx 0.02$ fs in the helium impact ionization. We also note that for these short beams the tunnel ionization is negligible.

In Fig. 4, we present the results for single ionization of He$(1s^2)$ by two long beams, each with $N_t = 1.5 \times 10^9$, $L = 3$ μm, and $a_0 = 20$ μm. (The associated beam currents

are ≃24 kA.) The density of the first beam reads

$$\rho = \frac{N_t e^{-R_\perp^2/a_0^2}}{\pi a_0^2 L} \begin{cases} 0; & \eta \le -\frac{\Delta L}{2} \text{ or } \eta \ge L + \frac{\Delta L}{2} \\ \frac{1}{2}\left(1 + \sin\left(\frac{\pi\eta}{\Delta L}\right)\right); & -\frac{\Delta L}{2} \le \eta \le \frac{\Delta L}{2} \\ 1; & \frac{\Delta L}{2} \le \eta \le L - \frac{\Delta L}{2} \\ \frac{1}{2}\left(1 - \sin\left(\frac{\pi(\eta - L)}{\Delta L}\right)\right); & L - \frac{\Delta L}{2} \le \eta \le L + \frac{\Delta L}{2}. \end{cases} \tag{8}$$

The form of the density profile of the second beam is basically as in Eq. (7), but, in addition, this beam has a spike with the density $\delta\rho \sim e^{-4\eta^2/(\delta L)^2} e^{-R_\perp^2/a_0^2}$, containing 2×10^7 electrons.

The cross sections for the coherent impact ionization by the first and second beams with $\Delta L = \delta L = 0.05$ μm are shown in Fig. 4 by the solid and dash-dotted curves, respectively. The figure also displays the cross section for the tunnel and overbarrier ionization [38], which is the same for both beams, and the cross section (4) for ionization by individual electrons.

The results displayed in Figs. 3 and 4 demonstrate that, when condition (i) or (ii) is fulfilled, the coherent impact ionization is an efficient mechanism which can strongly outperform the tunnel ionization and the ionization by individual electrons.

The latter process depends weakly ($\sim \ln\gamma$) on the impact energy as is inherent to the processes of ionization and bound-free e^+e^- pair production (see, e.g., Ref. [39]) in high-energy collisions with individual projectiles.

The tunnel cross section at sufficiently high energy is practically constant. This can be understood by noting that at very high impact energies the low-frequency part of the beam field and the beam velocity are practically independent of the impact energy. Therefore, neither the tunneling rate nor the time interval when tunneling can occur noticeably vary with the impact energy.

In contrast, the cross section for the coherent impact ionization depends on the energy rather strongly. In order to get insight into the origin of this dependence, let us consider the corresponding ionization probability. In Fig. 5, this probability is shown for single ionization of $\mathrm{He}(1s^2)$ by a Gaussian beam [see Eq. (7)] with $N_t = 2 \times 10^6$, $L = 0.06$ μm, and $a_0 = 1$ μm at electron impact energies of 100 MeV, 1 GeV, and 10 GeV. It is seen that the probability increases with the impact energy, especially strongly extending toward larger b.

The effective range of the projectile electron-atom interaction is determined by the adiabatic collision radius $R_0 \simeq \gamma/q_\parallel$. The analysis of the cross section [given by Eqs. (A7)–(A9) in End Matter] shows that the number $N_c(q_\parallel)$ of coherently interacting beam electrons is roughly given by $N_c(q_\parallel) \simeq N_t(R_0/a_0)^2 e^{-q_\parallel^2 L^2/16}$ and $N_c(q_\parallel) \simeq N_t e^{-q_\parallel^2 L^2/16}$ at $R_0 \ll a_0$ and $R_0 \gg a_0$, respectively. At $R_0 \ll a_0$, the growth of impact energy enlarges the transverse size $\simeq R_0$ of the effective coherence volume $\simeq R_0^2/q_\parallel$, increasing N_c, and the cross section scales as γ^4. At asymptotically high energies, $\gamma \gg q_\parallel a_0$, the effective

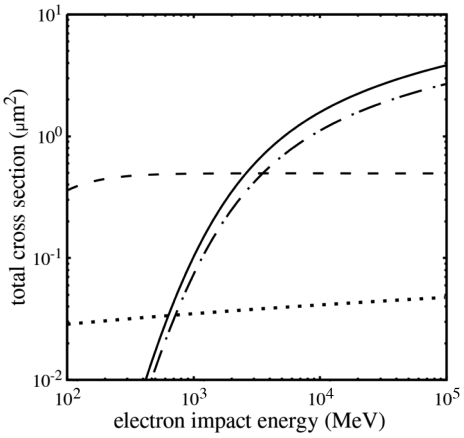


FIG. 4. Single ionization of $\mathrm{He}(1s^2)$ by beams with $N_t = 1.5 \times 10^9$, $L = 3$ μm ($L/v = 10$ fs), and $a_0 = 20$ μm. Solid and dash-dotted curves: the coherent impact ionization. Dashed curve: tunnel ionization. Dotted curve: the cross section (4). For more explanations, see the text.

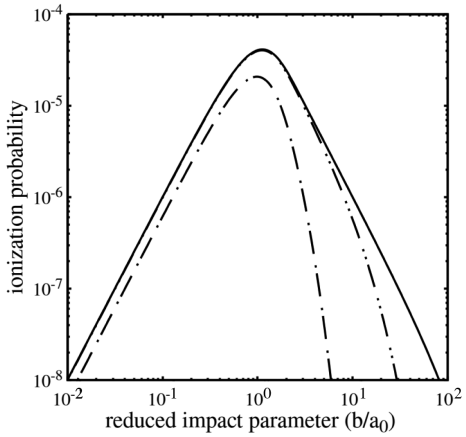


FIG. 5. The probability $P_{\mathrm{ion}}(b)$ for single ionization of $\mathrm{He}(1s^2)$ as a function of the position b of the atom with respect to the beam axis (see Fig. 1). $N_t = 2 \times 10^6$, $L = 0.06$ μm, and $a_0 = 1$ μm. Dash-dotted, dash-dotted-dotted, and solid curves: coherent impact ionization by 100 MeV, 1 GeV, and 10 GeV beams, respectively.

coherence volume is already bound by $\simeq a_0^2/q_\parallel$, and the cross section scales as $\ln\gamma$, which is similar to collisions with individual electrons.

In the total cross section, the coherent impact ionization strongly dominates ionization by individual electrons if $N_t \gg (q_\parallel^{\rm th} a_0/\gamma)^4 e^{(q_\parallel^{\rm th} L)^2/8}\alpha_1 \ln(\alpha_2 \gamma v/v_B)$ and $N_t \gg e^{(q_\parallel^{\rm th} L)^2/8}$ at $\gamma \ll q_\parallel^{\rm th} a_0$ and $\gamma \gg q_\parallel^{\rm th} a_0$, respectively, where $q_\parallel^{\rm th} = |\varepsilon_i|/v$.

The tunnel ionization is also very sensitive to the beam parameters. However, while the coherent impact ionization is especially sensitive to the longitudinal profile of the beam (determining the energy distribution of the equivalent photons), the tunneling very strongly depends on its transverse profile and the quantity N_t/L [both influence the beam field strength F to which the tunneling ionization rate $\sim(F_a/F)\exp(-2F_a/3F)$, where $F_a \sim 10^9$ V/cm is the characteristic atomic field, is extremely sensitive].

Beam shape and energy spread—In our consideration, the beam is taken as monochromatic and its shape (a_0, L) is supposed to change little when the beam penetrates the target. As our estimates show, for the parameters N_t, a_0, and L used in Figs. 3–5 and a target size of $\lesssim 1$ cm [40], this is the case if $D \lesssim (m_e c^2 a_0^2/N_t e_0^2)\gamma$, where D is the distance between the place where the beam was formed and the target [41]. For 1, 10, and 100 GeV electrons, this yields $D \lesssim 0.4$ m, $\lesssim 4$ m, and $\lesssim 40$ m, respectively.

The relative energy spread of the beams typically varies between 0.01 and 0.1 [42], which has no significant impact on the calculated cross sections [43]. This spread corresponds to a "longitudinal" temperature of $\simeq$10–1000 eV in the beam rest frame. In that frame, the densities of beams considered in Figs. 3–5 do not exceed 5×10^{16} cm^{-3}. As a result, the available phase space per electron greatly exceeds $(2\pi\hbar)^3$ and the fermionic nature of the beam electrons plays no role.

Target size and screening effects—The growth of the impact cross section(s) with the collision energy is eventually limited either by the transverse size of the target (we assume that it is much larger than the beam radius a_0) and/or by the target density effect, in which atoms closer to the projectile trajectory shield the projectile field for atoms farther away. Both these effects were omitted in our consideration, which is justified when the transverse size $d_{\rm tr}$ of the gas target greatly exceeds the adiabatic collision radius R_0 and the target density is sufficiently low (see, e.g., Refs. [34,44]). At the impact energies considered in Figs. 3 and 4, $R_0 \lesssim 1$ mm. Thus, the target size effect will be unimportant if $d_{\rm tr} \gtrsim 5$ mm, and, as our estimates show, even at 100 GeV the cross sections are still unaffected by the density effect, if the helium density $\lesssim 10^{13}$ cm^{-3}.

Ionization by secondary particles—The atoms can also be ionized by the electrons, emitted due to the interaction with the beam, and by the bremsstrahlung radiation. However, our estimates show that the former can be neglected for helium densities $\lesssim 10^{17}$ cm^{-3}, whereas the latter is negligible for any possible helium density. Our estimates also show that the radiation by the electron beam during the "preparatory stage" (where the beam is focused, compressed, or bent) will not noticeably ionize the target due to (i) a very small size of the latter, (ii) insufficient focusing of this radiation, and (iii) its very broad spectrum extending to large photon energies ($\gtrsim$100 eV) where the helium photo ionization is inefficient [45,46].

Electron beams with the parameters considered in Figs. 3–5 create in the lab frame electromagnetic fields whose strength does not significantly exceed $\sim$0.1 a.u. $= 5 \times 10^8$ V/cm. In this frame, the transverse ($\perp \boldsymbol{v}$) component of the Lorentz force acting on the beam electrons does not exceed $\sim 0.1/\gamma^2$ a.u. and its longitudinal component $\ll 0.1$ a.u. Such fields influence rather modestly beam and atomic electrons (the latter can be seen in Fig. 5, where the ionization probability remains always well below 10^{-4}). They also do not lead to any significant emission of radiation, making completely negligible the radiation reaction force [47].

In conclusion, we have predicted and explored a mechanism of impact ionization by high-density compact beams of extreme relativistic electrons, in which a significant fraction of these electrons coherently interacts with the atom. We have compared it with another coherent mechanism, the tunnel and overbarrier ionization, and with ionization by the incoherent action of individual beam electrons, showing that it can strongly dominate the ionization process.

We have also demonstrated that this mechanism possesses interesting physical peculiarities and, like the tunnel ionization, is highly sensitive to the spatiotemporal structure of the beam, which makes its account necessary for analyzing the beam properties.

Acknowledgments—We thank B. Najjari, B. Hidding, T. Heinemann, L. Reichwein, and A. Pukhov for useful discussions. S. K. gratefully acknowledges funding by the Studienstiftung des deutschen Volkes.

Data availability—The data that support the findings of this article are not publicly available upon publication because it is not technically feasible and/or the cost of preparing, depositing, and hosting the data would be prohibitive within the terms of this research project. The data are available from the authors upon reasonable request.

[1] R. E. Taylor, Deep inelastic scattering: The early years, Rev. Mod. Phys. **63**, 573 (1991).
[2] D. S. Armstrong and R. D. McKeown, Parity-violating electron scattering and the electric and magnetic strange form factors of the nucleon, Annu. Rev. Nucl. Part. Sci. **62**, 337 (2012).
[3] J. Arrington, N. Fomin, and A. Schmidt, Progress in understanding short-range structure in nuclei: An experimental perspective, Annu. Rev. Nucl. Part. Sci. **72**, 307 (2022).
[4] V. Shiltsev and F. Zimmermann, Modern and future colliders, Rev. Mod. Phys. **93**, 015006 (2021).

[5] A. Novikova, Probing matter with relativistic electron beams, Nat. Rev. Phys. **1**, 363 (2019).
[6] J. Feldhaus, J. Arthur, and J. B. Hastings, X-ray free-electron lasers, J. Phys. B **38**, S799 (2005).
[7] C. Pellegrini, A. Marinelli, and S. Reiche, The physics of x-ray free-electron lasers, Rev. Mod. Phys. **88**, 015006 (2016).
[8] M. C. Downer, R. Zgadzaj, A. Debus, U. Schramm, and M. C. Kaluza, Diagnostics for plasma-based electron accelerators, Rev. Mod. Phys. **90**, 035002 (2018).
[9] E. Esarey, C. B. Schroeder, and W. P. Leemans, Physics of laser-driven plasma-based electron accelerators, Rev. Mod. Phys. **81**, 1229 (2009).
[10] T. Tajima, X. Q. Yan, and T. Ebisuzaki, Wakefield acceleration, Rev. Mod. Plasma Phys. **4**, 7 (2020).
[11] E. Gschwendtner and P. Muggli, Plasma wakefield accelerators, Nat. Rev. Phys. **1**, 246 (2019).
[12] C. A. Lindstrøm, S. Corde, R. D'Arcy, S. Gessner, M. Gilljohann, M. J. Hogan, and J. Osterhoff, Beam-driven plasma-wakefield acceleration, arXiv:2504.05558.
[13] J. P. Couperus, R. Pausch, A. Köhler, O. Zarini, J. M. Krämer, M. Garten, A. Huebl, R. Gebhardt, U. Helbig, S. Bock, K. Zeil, A. Debus, M. Bussmann, U. Schramm, and A. Irman, Demonstration of a beam loaded nanocoulomb-class laser wakefield accelerator, Nat. Commun. **8**, 487 (2017).
[14] C. Emma, N. Majernik, K. K. Swanson, R. Ariniello, S. Gessner, R. Hessami, M. J. Hogan, A. Knetsch, K. A. Larsen, A. Marinelli, B. O'Shea, S. Perez, I. Rajkovic, R. Robles, D. Storey, and G. Yocky, Experimental generation of extreme electron beams for advanced accelerator applications, Phys. Rev. Lett. **134**, 085001 (2025).
[15] A. F. Habib, Th. Heinemann, G. G. Manahan, D. Ullmann, P. Scherkl, A. Knetsch, A. Sutherland, A. Beaton, D. Campbell, L. Rutherford *et al.*, Plasma photocathodes, Ann. Phys. (Berlin) **535**, 2200655 (2023).
[16] A. Deng, O. S. Karger, T. Heinemann, A. Knetsch, P. Scherkl, G. G. Manahan, A. Beaton, D. Ullmann, G. Wittig, A. F. Habib *et al.*, Generation and acceleration of electron bunches from a plasma photocathode, Nat. Phys. **15**, 1156 (2019).
[17] A. F. Habib, G. G. Manahan, P. Scherkl, T. Heinemann, A. Sutherland, R. Altuiri, B. M. Alotaibi, M. Litos, J. Cary, T. Raubenheimer *et al.*, Attosecond-Angstrom free-electron-laser towards the cold beam limit, Nat. Commun. **14**, 1054 (2023).
[18] J. B. Rosenzweig, G. Andonian, P. Bucksbaum, M. Ferrario, S. Full, A. Fukusawa, E. Hemsing, B. Hidding, M. Hogan, P. Krejcik, P. Muggli, G. Marcus, A. Marinelli, P. Musumeci, B. O'Shea, C. Pellegrini, D. Schiller, and G. Travish, Teravolt-per-meter beam and plasma fields from low-charge femtosecond electron beams, Nucl. Instrum. Methods Phys. Res., Sect. A **653**, 98 (2011).
[19] S. Kuschel *et al.*, Demonstration of passive plasma lensing of a laser wakefield accelerated electron bunch, Phys. Rev. Accel. Beams **19**, 071301 (2016).
[20] C. Thaury, E. Guillaume, A. Döpp, R. Lehe, A. Lifschitz, K. Ta Phuoc, J. Gautier, J.-P. Goddet, A. Tafzi, A. Flacco *et al.*, Demonstration of relativistic electron beam focusing by a laser-plasma lens, Nat. Commun. **6**, 6860 (2015).
[21] C. E. Doss, E. Adli, R. Ariniello, J. Cary, S. Corde, B. Hidding, M. J. Hogan, K. Hunt-Stone, C. Joshi, K. A. Marsh *et al.*, Laser-ionized, beam-driven, underdense, passive thin plasma lens, Phys. Rev. Accel. Beams **22**, 111001 (2019).
[22] Y.-Y. Chang, J. C. Cabadağ, A. Debus, A. Ghaith, M. LaBerge, R. Pausch, S. Schöbel, P. Ufer, U. Schramm, and A. Irman, Reduction of the electron-beam divergence of laser wakefield accelerators by integrated plasma lenses, Phys. Rev. Appl. **20**, L061001 (2023).
[23] E. G. Gelfer, A. M. Fedotov, O. Klimo, and S. Weber, Coherent radiation of an electron bunch colliding with an intense laser pulse, Phys. Rev. Res. **6**, L032013 (2024).
[24] M. J. Quin, A. Di Piazza, and M. Tamburini, Coherent frequency combs from electrons colliding with a laser pulse, Plasma Phys. Controlled Fusion **67**, 055008 (2025).
[25] We have also performed calculations by describing beam electrons by Dirac plane-wave states. After the averaging over spin states of the incident electron and summing over spin states of the scattered electron (taking into account that the scattering angle is very small), the resulting cross sections fully coincide with those which are obtained by using the semiclassical approach.
[26] J. Eichler, *Lectures on Ion-Atom Collisions* (Elsevier, New York 2005).
[27] R. Moshammer, W. Schmitt, J. Ullrich, H. Kollmus, A. Cassimi, R. Dörner, O. Jagutzki, R. Mann, R. E. Olson *et al.*, Ionization of helium in the attosecond equivalent light pulse of 1 GeV/Nucleon U^{92+} projectiles, Phys. Rev. Lett. **79**, 3621 (1997).
[28] A. B. Voitkiv, B. Najjari, R. Moshammer, and J. Ullrich, Helium single ionization in relativistic collisions with highly charged ions, Phys. Rev. A **65**, 032707 (2002); A. B. Voitkiv and B. Najjari, Ionization of helium by relativistic highly charged ions within the symmetric eikonal approximation, J. Phys. B **37**, 4831 (2004).
[29] $\lambda_{\parallel}$ and $\lambda_{\perp}$ can be viewed as the longitudinal and transverse wavelengths, respectively, of the equivalent photon.
[30] A. B. Voitkiv and J. Ullrich, On the inter-relation between ionization of light atoms by virtual and real photons, J. Phys. B **34**, 4513 (2001).
[31] For instance, for single ionization of He$(1s^2)$ $\alpha_1 = 12.289$ and $\alpha_2 = 2.08$ [32].
[32] M. Inokuti, Inelastic collisions of fast charged particles with atoms and molecules-the Bethe theory revisited, Rev. Mod. Phys. **43**, 297 (1972); **50**, 23 (1978).
[33] E. Fermi, Über die Theorie des Stoßes zwischen Atomen und elektrisch geladenen Teilchen, Z. Phys. **29**, 315 (1924); C. F. von Weizsäcker, Ausstrahlung bei Stößen sehr schneller Elektronen, Z. Phys. **88**, 612 (1934); E. J. Williams, Nature of the high energy particles of penetrating radiation and status of ionization and radiation formulae, Phys. Rev. **45**, 729 (1934).
[34] J. D. Jackson, *Classical Electrodynamics*, 3rd ed., (Wiley, New York, 1999).
[35] L. D. Landau and E. M. Lifshitz, *Quantum Mechanics* (Pergamon, New York, 1965).
[36] M. V. Ammosov, N. B. Delone, and V. P. Krainov, Tunnel ionization of complex atoms and of atomic ions in an alternating electromagnetic field, Zh. Eksp. Teor. Fiz. **91**, 2008 (1986) [Sov. Phys. JETP **64**, 1191 (1987)].
[37] G. G. Manahan, A. Deng, O. Karger, Y. Xi, A. Knetsch, M. Litos, G. Wittig, T. Heinemann, J. Smith, Z. M. Sheng,

D. A. Jaroszynski, G. Andonian, D. L. Bruhwiler, J. B. Rosenzweig, and B. Hidding, Hot spots and dark current in advanced plasma wakefield accelerators, Phys. Rev. Accel. Beams **19**, 011303 (2016).
[38] See End Matter.
[39] A. B. Voitkiv, Basic atomic processes in high-energy ion–atom collisions, in *Springer Handbook of Atomic, Molecular, and Optical Physics*, 2nd ed., edited by Gordon W. F. Drake (Springer, New York, 2023), Chap. 57.
[40] We note that a typical size of a gas target in experiments on fast electron-atom and ion-atom collisions does not exceed several millimeters.
[41] In this estimate, a normalized emittance of $\epsilon_n = 0.5$ mm · mrad was assumed.
[42] T. Heinemann and B. Hidding (private communication).
[43] Our estimates show that the effect of the beam energy spread and fluctuation on the cross section can be neglected if $\Delta E/E = \Delta\gamma/\gamma \ll 1$, where $E = m_e c^2\gamma$ and $\Delta E = m_e c^2\Delta\gamma$ are the mean electron energy and its spread or fluctuation, respectively.
[44] L. D. Landau and E. M. Lifshitz, *Electrodynamics of Continuous Media* (Pergamon Press, New York, 1984), see Sec. 85.
[45] To illustrate items (i)–(iii), we note the following. Suppose that an electron beam, which moves along the z axis, enters a magnetic field B_0, which is perpendicular to this axis and acts on a distance l_0 along it. Then, at a distance D downstream from the magnetic field, the radiation, which was emitted by the beam in this field, will spread over the area $S \simeq \pi(l_0 + D)^2(e_0 B_0 l_0/m_e c^2\gamma)^2$. For instance, at $\gamma = 2000$, $B_0 \simeq 1$ T, $l_0 \simeq 1$ m, and $D \simeq 1$ m, we obtain $S \simeq 1\,\mathrm{m}^2$. This is about 10^4–10^5 times larger than the area $s_0 \simeq 10$–100 mm^2 of a typical gas target used in experiments on ionization by fast projectiles, meaning that essentially all emitted radiation misses the target. Moreover, the spectrum of the radiation spreads over a very broad energy range, maximizing at about 700 eV. Such energies are large on the scale of helium atoms, which means that the radiation would not be efficient in ionizing helium atoms even if a significant fraction of it would penetrate the target.
[46] Radiation occurs also when the electron beam is produced inside a plasma. However, the fields acting on the electrons are there so strong (effectively corresponding to magnetic fields of $\sim 10^3$ T) that the spectrum of the emitted radiation is in the range of $\sim$100 keV–1 MeV. Such radiation cannot be absorbed by light atoms and can ionize them only via Compton scattering whose cross section is very small ($\lesssim 10^{-24}$ cm^2), making this process unimportant for target ionization.
[47] A. Gonoskov, T. G. Blackburn, M. Marklund, and S. S. Bulanov, Charged particle motion and radiation in strong electromagnetic fields, Rev. Mod. Phys. **94**, 045001 (2022).
[48] M. Abramowitz and I. Stegun, *Handbook of Mathematical Functions* (Dover Publications, Inc., New York, 1965).
[49] F. Martin and A. Salin, Accurate evaluation of multiple-excitation cross sections from one-electron amplitudes, Phys. Rev. A **55**, 2004 (1997).
[50] S. Remme, A. B. Voitkiv, G. Pretzler, and C. Müller, Phenomenological rate formulas for over-barrier ionization of hydrogen and helium atoms in strong constant electric fields, J. Phys. B **58**, 195602 (2025); X. M. Tong and C. D. Lin, Empirical formula for static field ionization rates of atoms and molecules by lasers in the barrier-suppression regime, J. Phys. B **38**, 2593 (2005).
[51] A. Scrinzi, M. Geissler, and T. Brabec, Ionization above the Coulomb barrier, Phys. Rev. Lett. **83**, 706 (1999).

End Matter

Coherent impact ionization—Within the first order of the perturbation in the interaction between the atom and the jth beam electron, the atomic transition amplitude in the impact parameter space is given by

$$a_{fi}^{j}(\boldsymbol{b}) = -\frac{i}{\hbar}\gamma e_0^2 \int_{-\infty}^{+\infty} dt e^{i\omega_{fi}t} \int d^3\boldsymbol{\xi}\varphi_f^*(\boldsymbol{\xi}) \times \left\{\frac{1}{D} - \frac{v}{2m_e c^2}\left(\frac{1}{D}\hat{p}_z + \hat{p}_z\frac{1}{D}\right)\right\}\varphi_i(\boldsymbol{\xi}). \tag{A1}$$

Here, $\boldsymbol{\xi}$ is the coordinate of the atomic electron with respect to the atomic nucleus, φ_i (ε_i) and φ_f (ε_f) are the initial and final states (energies), respectively, of the atomic electron, $\omega_{fi} = (\varepsilon_f - \varepsilon_i)/\hbar$ is the atomic transition frequency, $\hat{p}_z = (\hbar/i)(\partial/\partial\xi_z)$, and $D = \sqrt{(\boldsymbol{\xi}_\perp + \boldsymbol{b} - \boldsymbol{R}_\perp)^2 + \gamma^2[\xi_z - v(t - t_j)]^2}$.

By using the Fourier representation for the Lienard-Wiechert potentials (1), the amplitude (A1) can be transformed into

$$a_{fi}^{j}(\boldsymbol{b}) = -\frac{i}{\hbar}\frac{e_0^2}{\pi v} e^{iq_\parallel v t_j} \int \frac{d^2\boldsymbol{Q}_\perp e^{i\boldsymbol{Q}_\perp\cdot(\boldsymbol{b}-\boldsymbol{R}_{\perp j})}}{\boldsymbol{Q}_\perp^2 + q_\parallel^2/\gamma^2} \times \left\langle \varphi_f \middle| e^{i\boldsymbol{q}\cdot\boldsymbol{\xi}} - \frac{v}{2m_e c^2}\left(e^{i\boldsymbol{q}\cdot\boldsymbol{\xi}}\hat{p}_z + \hat{p}_z e^{i\boldsymbol{q}\cdot\boldsymbol{\xi}}\right)\middle| \varphi_i \right\rangle, \tag{A2}$$

where $\boldsymbol{q} = (\boldsymbol{Q}_\perp, q_\parallel)$ with $q_\parallel = \omega_{fi}/v$.

It is more convenient to calculate the transition amplitude in the momentum space where it is given by

$$S_{fi}^{j}(\boldsymbol{q}_\perp) = \frac{1}{2\pi}\int d^2\boldsymbol{b} a_{fi}^{j}(\boldsymbol{b}) e^{i\boldsymbol{q}_\perp\cdot\boldsymbol{b}} = -\frac{2i}{\hbar}\frac{e_0^2}{v} e^{iq_\parallel v t_j} e^{-i\boldsymbol{q}_\perp\cdot\boldsymbol{R}_{\perp j}} \frac{1}{\boldsymbol{q}'^2} \times \left\langle \varphi_f \middle| e^{i\boldsymbol{q}\cdot\boldsymbol{\xi}} - \frac{v}{2m_e c^2}\left(e^{i\boldsymbol{q}\cdot\boldsymbol{\xi}}\hat{p}_z + \hat{p}_z e^{i\boldsymbol{q}\cdot\boldsymbol{\xi}}\right)\middle| \varphi_i \right\rangle. \tag{A3}$$

Here, $\hbar\boldsymbol{q} = (\hbar\boldsymbol{q}_\perp, \hbar q_\parallel)$ $[\hbar\boldsymbol{q}' = (\hbar\boldsymbol{q}_\perp, \hbar q_\parallel/\gamma)]$ is the momentum transferred to the atom in the collision as

viewed in the laboratory frame (in the rest frame of the incident electron).

A generalization of the amplitude (A3) for atoms with more than one electron is elementary, yielding

$$S_{fi}^{j}(\boldsymbol{q}_\perp) = -\frac{2i}{\hbar}\frac{e_0^2}{v} e^{iq_\parallel v t_j} e^{-i\boldsymbol{q}_\perp\cdot\boldsymbol{R}_{\perp,j}} \frac{1}{\boldsymbol{q}'^2} \times \left\langle \varphi_f \left| \sum_{k=1}^{N_a} e^{i\boldsymbol{q}\cdot\boldsymbol{\xi}_k} \left(1 - \frac{v(\hbar q_\parallel + 2\hat{p}_{k,z})}{2m_e c^2}\right) \right| \varphi_i \right\rangle. \tag{A4}$$

Here, the sum runs over N_a atomic electrons and φ_i and φ_f depend on the set $(\boldsymbol{\xi}_1, \boldsymbol{\xi}_2, \ldots, \boldsymbol{\xi}_{N_a})$ of coordinates of atomic electrons.

The ionization cross section for the coherent impact ionization, differential in the energy ε_p and the solid angle Ω_p of the emitted electron, is obtained according to

$$\frac{d^2\sigma^{\mathrm{CII}}}{d\varepsilon_p d\Omega_p} = p \int d^2\boldsymbol{q}_\perp |S_{fi}(\boldsymbol{q}_\perp)|^2, \tag{A5}$$

where p is the momentum of the emitted electron.

Atomic ionization by highly relativistic ($\gamma \gg 1$) charged projectiles is dominated by collisions with small momentum transfers, $\hbar q \ll Q_a$, where Q_a is the characteristic electron momentum in the initial atomic state (see, e.g., Ref. [30]). Our calculations and the analysis of the cross section (A5) show that in the coherent impact ionization the dominance of collisions with small momentum transfers becomes overwhelming, and they practically entirely determine the ionization cross sections. This enables one to greatly simplify the consideration by calculating the transition amplitude $S_{fi}(\boldsymbol{q}_\perp)$ within the dipole approximation.

Taking the beam density as

$$\rho(\boldsymbol{R}, t) = \frac{2N_t}{\pi^{3/2} a_0^2 L} e^{-4(Z-vt)^2/L^2} e^{-R_\perp^2/a_0^2}, \tag{A6}$$

where L and a_0 are the effective beam length and radius, respectively (see Fig. 1), for ionization of an atom with one "active" electron initially in an s state we obtain

$$\frac{d^2\sigma^{\mathrm{CII}}}{d\varepsilon_p d\Omega_p} = p\frac{N_t^2}{v^2}\Lambda e^{-q_\parallel^2 L^2/8}\Sigma. \tag{A7}$$

Here, $\Lambda = (1/p^2)\left(\int_0^\infty d\xi \xi^3 R_{p,1}(\xi) R_i(\xi)\right)^2$, where R_i and $R_{p,1}$ are the radial wave functions of the initial and final (continuum) states, respectively, of the atomic electron [with $R_{p,1}$ being normalized according to $\int_0^\infty d\xi \xi^2 R_{p,1}(\xi) R_{p',1}(\xi) = \delta(p - p')$] and Σ reads

$$\Sigma = \frac{\cos^2\vartheta_p}{\gamma^2} F(y_0) + 0.5\sin^2\vartheta_p G(y_0), \tag{A8}$$

where ϑ_p is the polar electron emission angle, $q_\parallel = (\varepsilon_p - \varepsilon_i)/\hbar v$, $y_0 = 0.5(q_\parallel a_0/\gamma)^2$, and

$$F(y_0) = 1 - y_0 e^{y_0} E_1(y_0),$$
$$G(y_0) = e^{y_0} E_1(y_0)(1 + y_0) - 1 \tag{A9}$$

with E_1 being the exponential integral function [48].

The total cross section for coherent ionization is obtained by integrating (A7) over the solid angle and the emission energy.

Furthermore, for the beam density, given by Eq. (A6), and assuming $\gamma \gg 1$, we obtain that the ionization probability for the coherent impact ionization, differential in the electron emission energy, is given by

$$\frac{dP_{\mathrm{ion}}^{\mathrm{CII}}(b, \varepsilon_p)}{d\varepsilon_p} = \frac{16p}{3}\frac{N_t^2}{v^2}\Lambda e^{-q_\parallel^2 L^2/8}\left(q_\parallel \mathcal{M}_\perp(b)/\gamma\right)^2. \tag{A10}$$

Here,

$$\mathcal{M}_\perp(b) = K_1(q_\parallel b/\gamma)\int_0^{b/a_0} dx x e^{-x^2} I_0(q_\parallel a_0 x/\gamma) - I_1(q_\parallel b/\gamma)\int_{b/a_0}^\infty dx x e^{-x^2} K_0(q_\parallel a_0 x/\gamma), \tag{A11}$$

where I_0, I_1, K_0, and K_1 are the modified Bessel functions [48]. The ionization probability $P_{\mathrm{ion}}^{\mathrm{CII}}(b)$ is obtained by integrating (A10) over the electron emission energy.

In our consideration of collisions with helium atoms, we took into account that the total cross section for helium single ionization by fast projectiles is weakly influenced by correlation between the atomic electrons. The initial and final states were described by a properly symmetrized product of single-electron orbitals whose radial parts were computed numerically using the effective potential

$$V(\xi) = -\frac{1}{\xi} - (1 + \beta\xi)\frac{\exp(-\alpha\xi)}{\xi} \tag{A12}$$

with $\alpha = 3.36$ and $\beta = 1.665$ (see Ref. [49]) for the initial and final states, respectively. Using these states in the amplitude (A4) and employing the dipole approximation, we obtain that the ionization cross section is given by the rhs of Eq. (A7) [where now R_i and $R_{p,1}$ are computed by using the interaction (A12)] multiplied by a factor of 2, which arises due to two "identical" electrons in the ground helium state.

Coherent ionization via tunnel and overbarrier mechanisms—In order to calculate the total cross section and the probability for ionization via these mechanisms,

we first evaluated the strength $\boldsymbol{E}$ of the electric field created by the beam. In particular, for the beam density given by Eq. (A6), we obtained the following expression:

$$E_\perp(\boldsymbol{r},t)=\frac{N_t e_0}{2}\int_0^\infty dqqJ_1(qr_\perp)e^{-q^2a_0^2/4}e^{\gamma^2q^2l^2/4}\times\left\{e^{\gamma q\eta}[1-\mathrm{erf}(\gamma ql/2+\eta/l)]+e^{-\gamma q\eta}[1-\mathrm{erf}(\gamma ql/2-\eta/l)]\right\} \tag{B1}$$

and

$$E_z(\boldsymbol{r},t)=\frac{N_t e_0}{2\gamma}\int_0^\infty dqqJ_0(qr_\perp)e^{-q^2a_0^2/4}e^{\gamma^2q^2l^2/4}\times\left\{e^{\gamma q\eta}[1-\mathrm{erf}(\gamma ql/2+\eta/l)]-e^{-\gamma q\eta}[1-\mathrm{erf}(\gamma ql/2-\eta/l)]\right\}. \tag{B2}$$

Here, $E_\perp(\boldsymbol{r},t)$ and $E_z(\boldsymbol{r},t)$ are the transverse ($\boldsymbol{E}_\perp\perp\boldsymbol{v}$) and longitudinal ($E_z=\boldsymbol{E}\cdot\boldsymbol{v}/v$) components, respectively, of the field $\boldsymbol{E}$, $\boldsymbol{r}=(r_\perp,z)$ is the coordinate at which the field is calculated ($r_\perp$ is counted from the beam axis), $\eta=z-vt$, $l=L/2$, J_0 and J_1 are the Bessel functions, and erf is the error function (see Ref. [48]).

To calculate the cross sections for the tunneling and overbarrier ionization of helium, we have used empirical rate expressions from [50] which apply to ionization by a constant or slowly varying electric field.

In the regime of field strengths $F\le 0.42$ a.u. (corresponding to about twice the barrier-suppression field $F_c=I_p^2/4$), we employ the formula

$$W_{\text{near-OBI}}=W_{\text{TI}}(F,\kappa)\exp\left(a_1\frac{F^2}{F_c^2}+a_2\frac{F}{F_c}+a_3\right), \tag{B3}$$

where

$$W_{\text{TI}}(F,\kappa)=\frac{C_a^2}{2\kappa^{2/\kappa-1}}\left(\frac{2\kappa^3}{F}\right)^{2/\kappa-1}\exp\left(-\frac{2\kappa^3}{3F}\right) \tag{B4}$$

denotes the Ammosov-Delone-Krainov (ADK) tunneling rate of helium, with $C_a=2.67$, $\kappa=\sqrt{2I_p}$, and the binding potential $I_p=0.904$ a.u. The ADK rate is amended in Eq. (B3) by an exponential factor, which accounts for the Stark effect and a widened electron emission angle. It contains the fit parameters $a_1=0.042\,177$, $a_2=-0.762\,430$, and $a_3=0.039\,149$.

At higher fields $F>0.42$ a.u., we use the formula

$$W_{\text{far-OBI}}=\frac{aF^b}{c+F^d}, \tag{B5}$$

with $a=1.115\,21$, $b=3.460\,03$, $c=0.353\,54$, and $d=2.233\,55$. The free parameters in Eqs. (B3) and (B5) have been determined by fitting to numerical ionization rates from [51].

All further technical details of our calculations of the cross sections and the ionization probabilities for the coherent impact and tunnel (or overbarrier) ionization will be reported in a forthcoming paper.